Chapter 14
Recognition Enhancement of Dementia Patients' Working Memory Using Entropy-Based Features and Local Tangent Space Alignment Algorithm

Noor Kamal Al-Qazzaz, Sawal Hamid Bin Mohd Ali, and Siti Anom Ahmad

Abstract Detecting dementia presents a barrier to advancing individualized healthcare. Electroencephalographic (EEG) signals' nonlinear nature has been characterized using entropies. While a working memory (*WM*), the EEGs of 5 patients suffering vascular dementia (*VD*), 15 patients had stroke-related mild cognitive impairment (*SMCI*), and 15 healthy normal control (*NC*) participants were evaluated in this study. A four-step framework for the automatic identification of dementia is provided, with the first stage employing the newly developed automatic independent component analysis and wavelet (AICA-WT) method. In the second stage, nonlinear entropy features using fuzzy entropy (*FuzzEn*), fluctuation-based dispersion entropy (*FDispEn*), and bubble entropy (*BubbEn*) were utilized to extract various dynamical properties from multi-channel EEG signals derived from patients with dementia. A statistical examination of the individual performance was conducted using analysis of variance (ANOVA) to determine the degree of EEG complexity across brain regions. Afterwards, the nonlinear local tangent space alignment (LSTA) dimensionality reduction approach was utilized to enhance the automatic

N. K. Al-Qazzaz (✉)
Department of Biomedical Engineering, Al-Khwarizmi College of Engineering, University of Baghdad, Baghdad, Iraq
e-mail: noorbme@kecbu.uobaghdad.edu.iq

Sawal Hamid Bin Mohd Ali
Department of Electrical, Electronic & Systems Engineering, Faculty of Engineering & Built Environment, Universiti Kebangsaan Malaysia, UKM Bangi, Bangi, Selangor, Malaysia
e-mail: sawal@ukm.edu.my

S. A. Ahmad
Department of Electrical and Electronic Engineering, Faculty of Engineering, Universiti Putra Malaysia, UPM Serdang, Serdang, Selangor, Malaysia

Malaysian Research Institute of Ageing (MyAgeing™), Universiti Putra Malaysia, Serdang, Serdang, Selangor, Malaysia
e-mail: sanom@upm.edu.my

S. Mian Qaisar et al. (eds.), *Advances in Non-Invasive Biomedical Signal Sensing and Processing with Machine Learning*, https://doi.org/10.1007/978-3-031-23239-8_14

diagnosis of dementia patients'. Using *k*-nearest neighbors (*k*NN), support vector machine (*SVM*), and decision tree (*DT*) classifiers, the impairment of post-stroke patients was finally identified. BubbEn is chosen to develop a new *BubbEn*-LTSA mapping process for creating the innovative AICA-WT-*BubbEn*-LTSA dementia recognition framework, which is the basis for an automated VD detection.

14.1 Introduction

Cognitive impairment and dementia are progressive impairments of mental function that are frequent following a stroke and inevitably lead to limitations in independent life. It was estimated that 50 million individuals were affected globally in 2018, and by 2050, that number is anticipated to triple [1]. After Alzheimer's disease (*AD*), vascular dementia (*VD*) is the second most prevalent type of dementia, and its prevalence doubles every 5–10 years after age 65 [2–4]. The majority of people with vascular dementia are elderly adults over the age of 65. Clinically speaking, a reduction in mental ability that is higher than would be predicted given the people's age and education level but does not severely affect everyday activities is known as mild cognitive impairment (*MCI*) [5]. It's frequently thought of as being in the middle of the spectrum between early-on-normal brain cognition and late-on-severe dementia. Following a stroke diagnosis, the cognitive function most impacted by dementia and cognitive loss is memory [6, 7].

Better therapeutic therapy prior to brain damage from dementia would require earlier diagnosis. Early dementia diagnosis will help dementia patients start symptom-based treatment as quickly as possible. Recent years have seen significant advancements in the use of biomarkers to detect dementia in its earliest stages [8–11].

The use of magnetoencephalography (MEG) to record the brain activity of Alzheimer's disease (AD) patients has gained significant research interest over the past 20 years [12–15]. EEG is a therapeutic tool that has a high level of temporal resolution and can monitor brain activity in milliseconds [16]. Therefore, it is frequently used to establish a thorough study of a time-sensitive neurodynamic marker that assists in monitoring the brain for irregularities linked to cognitive decline and dementia [16, 17]. It can be used in neurophysiology to recognize and classify changes in the brain [18]. It is essential to develop a mechanism for detecting dementia in its early stages so that an ideal diagnostic index can be derived.

In this study, 15 healthy normal control (*NC*) volunteers, 15 patients with mild cognitive impairment (*SMCI*) following a stroke, and 5 patients with vascular dementia (*VD*) were used as *NC* to measure the background EEG activity during a working memory (WM) test. In the first step of a four-stage framework for the automatic identification of dementia, conventional filters with, a revolutionary automatic independent component analysis and wavelet (AICA-WT) approach was used. In the second stage, nonlinear entropy features such as fuzzy entropy (*FuzzEn*), fluctuation-based dispersion entropy (*FDispEn*), and bubble entropy (*BubbEn*) were utilized to extract various dynamical properties from multi-channel EEG signals derived from patients with dementia. The level of EEG complexity across brain areas was assessed statistically using analysis of variance (ANOVA) of the individual performance of estimated entropies. Afterwards, the nonlinear local tangent space alignment (LTSA) dimensionality reduction approach was utilized to enhance the automatic diagnosis of dementia patients' onset. Using $k - nearest$ *neighbors* (*k*NN), support vector machine (*SVM*), and decision tree (*DT*) classifiers, the disabilities suffered by stroke survivors was finally identified. The comparative efficiency of the LTSA method for scaling down data dimensions with the *k*NN, *SVM*, and *DT* classifiers has been examined. LTSA with *k*NN achieved the highest classification accuracies for *VD*, *SMCI*, and *NC*, respectively.

According to the author's knowledge, this is the first time such an analysis has been performed for dementia-based discriminative processing of EEG information. The initial contribution of this research is the proposal of an novel EEG AICA-WT-*BubbEn*-LTSA mapping architecture to improve early dementia identification. The suggested framework uses the novel AICA-WT denoising method and bubble entropy to stabilize complexity parameters. The performance of the proposed framework with three class classification tasks was acquired utilizing three distinct machine learning models in order to provide dependable classification performance and demonstrate the robustness of our proposed mapping framework. The working memory methodology for capturing EEG signals from *VD*, *SMCI*, and *NC* subjects is the first to interpret graphical behavior from EEG-based background activity. Novel AICA-WT-*BubbEn*-LTSA could be a core for automated *VD* detection and a promising, highly efficient technique for identifying *VD* and *SMCI* impaired effects on neuroelectrography alterations.

14.2 Related Works

Brain disorders like epilepsy, researchers have used EEG readings to diagnose both attention deficit hyperactivity disorder (*ADHD*) and *AD*. Using an EEG dataset with several channels spanning brain areas, it may be possible to evaluate a wide range of affective reactions. [4, 19–24]. Therefore, studies have demonstrated the potential for EEG signals to detect vascular dementia (*VD*) patients by examining working memory tasks and displaying brain alterations collected based on non-conscious EEG brainwave patterns in people with dementia [25, 26]. However, EEG data are typically polluted by motion, ocular, muscular, and cardiac activities [19, 27]. Greater magnitude artifacts distort the signal and mislead the analysis.

There is a growing body of research aimed at removing non-cerebral sources from EEG data, known as artifacts, which may imitate brain disease activity and so affect the analysis [19, 26]. Early techniques for detecting and removing artifacts included blind source separation (*BSS*) based on Independent Component Analysis (ICA) [28], wavelet denoising [29, 30] to enhance the performance [31]. However, wavelets are time-frequency spectrums that overlap, but ICA lacks redundancy in the number of signals relative to the number of sources. Al-Qazzaz [19, 32] have proposed the combination of ICA and wavelets approaches to solve these constraints.

In addition to being extremely informative on brain physiology, EEG signals may also serve as biomarkers of brain behavior [33–37]. The Hurst exponent (*Hur*) [32, 38] and fractal dimension (*FD*) [39, 40] nonlinear methods that have been used to represent and analyze cerebral cortex-generated complex dynamic data [41, 42]. Nonlinear parametric index of entropy can be used to quantify the uncertainty of dynamic systems like EEG signals that lack stability [43]. The field of cognitive neuroscience, sleep research, and the classification of emotional states have all profited from the use of entropy with EEG information [26, 40, 44, 45].

Entropy methods have been proposed throughout the previous three decades as a potent metric for quantifying the dynamic complexity of real-world systems such as EEG time series [43]. Entropies have been used to research cognitive thinking states, sleep states, and emotional level categorization techniques using the EEG signal [26, 40, 44, 45]. In addition, social emotion, personal identification, therapy uptake, clinical efficacy, and side effects are potential therapeutic uses of EEG-based biological gender recognition leveraging several entropies. [46]. Wang [47] employed *sample entropy* (*SampEn*), *approximate entropy* (*ApEn*), and *permutation entropy* (*PerEn*) to examine the human emotions in response to video clips due to the robustness of these entropies to noise and their ability to effectively assess the complexity of a time series [48, 49]. Researchers have proposed *fuzzy entropy* (*FuzzEn*) for EEG assessment. In addition, *Shannon entropy* (*ShEn*) and *conditional entropy* (*ConEn*) represent the amount of information and the rate at which new information is being made [50]. The widely-used *SampEn* is derived from *ConEn* [51], whereas *PerEn* and the newly developed *dispersion entropy* (*DispEn*) [52] are derived from *ShEn* [53]. *SampEn* gives unreliable or unknown entropy values for short time series and is inadequate for long signals [14, 15]. *PerEn* is intuitive and computationally efficient. However, it has a continuous distribution and is noise-sensitive. Fluctuation-based dispersion entropy (*FDispEn*) was proposed in [50] and Bubble entropy (*BubbEn*) was utilized in [54] to examine the dynamics of time series, specifically the distribution of symbol sequences, in order to address the inadequacies of *PerEn* and *SampEn*.

The advantage of this work is to find out how psychological EEG signals in different parts of the brain differ between *VD*, *SMCI*, and *NC* people by utilizing EEG markers to detect various dynamical features of dementia-based EEG background activity. Therefore, among the several empirical entropies, the *FuzzEn* [55], *FDispEn* [50] and *BubbEn* [54] entropies were chosen because they are noise-resistant and may provide important information for interpreting the time series complexity.

Methods like sequential feed-forward selection (*SFFS*), minimum redundancy maximum relevance (*mRMR*), genetic algorithm (*GA*), evolutionary computation (*EC*), and sparse discriminative ensemble learning (*SDEL*) algorithm, sparse linear discriminant analysis (LDA) and principle component analysis (*PCA*) have all been used to estimate the best features [56–61].

Xie [33] have utilized the *k*NN and *SVM* classifiers for seizure detection, whereas Subasi [62] have employed *PCA* as a dimensionality reduction technique and the *SVM* classifier with two outputs, either an epileptic seizure or not. In addition, for Brain Computer Interface (BCI) system applications, Vidaurre [63] examined brainwaves using a linear discriminant analysis (*LDA*) classifier, whereas Murugappan [64] classified discrete emotions using *k*NN and *LDA*. In addition, Lagun [65] categorised the EEG datasets of AD, *SMCI*, and NC participants using logistic regression (LR), naive Bayes (NB), and support vector machine (*SVM*). Chaovalitwongse [66] have presented a technique for classifying and detecting seizure precursors using *k*NN.

The majority of dementia detection investigations used EEG signals based on *AD*, and they concentrated on linear analysis employing spectral relative powers [67–69]. However, other studies [21, 70, 71] have employed nonlinear entropy characteristics to examine brain complexity behavior. To this goal, entropy features were computed to emphasize the diversity of dementia in affective-based EEG systems.

14.3 Methods and Materials

The recorded EEG requires several stages of signal processing and analysis in order to obtain relevant details from the EEG signal of *VD* and *SMCI* patients in order to enhance the accuracy of the diagnosis of degenerative changes. EEG may have a significant role in the diagnosis and severity categorization of dementia. Preprocessing, feature extraction, dimensionality reduction, and classification are the primary stages of EEG signal processing. Fig. 14.1 depicts the complexity of EEG processing algorithms.

14.3.1 Participants and EEG Recording

The *NicoletOne* (*V*32) system, developed and manufactured by *VIASYS* Healthcare Inc. in the United States, was used to gather the EEG data. The scalp was covered with 19 electrodes (including *ground* and system *reference* electrodes) in a cap electrode configuration. Here are the cutoff frequencies for the low-pass filter (*LPF*), high-pass filter (*HPF*), and notch hardware filters included in the EEG device: The 3 dB point for the LPF is at a frequency of 0.3 Hz, and the 70 Hz HPF upper cutoff frequency is adjustable. Typically, the notch filter is set at 50 Hz, and the frequency range is (0.3 to 70) Hz. The sampling frequency is determined by the application to be 256 Hz, etc., and a 12 *bit A*/*D* converter accurately digitizes the signal. 15 *NC* records, 15 *SMCI* patients, and 5 *VD* patients had their EEG data reviewed for this investigation. The participants serving as *NC* had no history of mental or neurological problems. The stroke patients were recruited from the *stroke ward* at *Pusat Perubatan Universiti Kebangsaan Malaysia* (*PPUKM*), the National University of

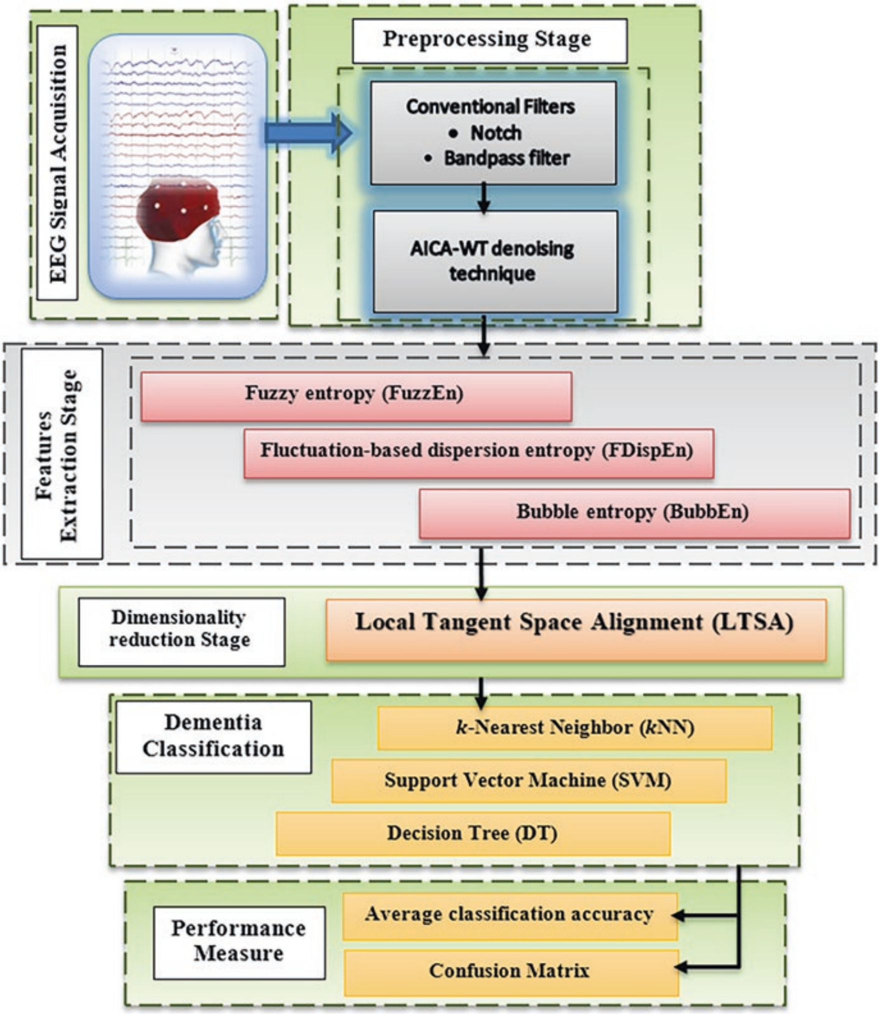

Fig. 14.1 The block diagram of current study

Malaysia's medical facility. Patients with *VD* were recruited through the *Neurology Clinic*. The stroke patient met the requirements of the *National Institutes of Health Stroke Scale* (*NIHSS*) [72]. All patients were diagnosed using magnetic resonance imaging (*MRI*) images of the brain, patient medical histories, and clinical and laboratory tests. The healthy *NC* group had no history of mental or neurological disorders. The *Mini – Mental State Examination* (*MMSE*) [73] and the *Montreal Cognitive Assessment* (*MoCA*) [74] were used to evaluate the cognitive abilities of both groups. In accordance with the 10–20 worldwide system, a total of 19 *electrodes* plus the *ground* and system reference electrode were placed (*Fp*1, *Fp*2, *F*7, *F*3, *Fz*, *F*4, *F*8, *T*3, *T*5, *T*4, *T*6, *P*3, *Pz*, *P*4, *C*3, *Cz*, *C*4, *O*1, *and O*2). Table 14.1

Table 14.1 Sociodemographic characteristics of the NC subjects and SMCI and VD patients.

Participant features	*NC*	*SMCI*	*VD*
Number	15	15	5
Age	60.06 ± 5.21	60.26 ± 7.77	64.6 ± 4.8
MMSE	29.6 ± 0.73	20.2 ± 5.63	14.8 ± 1.92
MoCA	29.06 ± 0.88	16.13 ± 5.97	13.2 ± 2.38
Gender	8 *Females*/7 *Males*	10 *Females*/5 *Males*	2 *Females*/3 *Males*

Age in years, MMSE Mini-Mental State Examination, MoCA Montreal Cognitive Assessment, SD meanstandard deviation

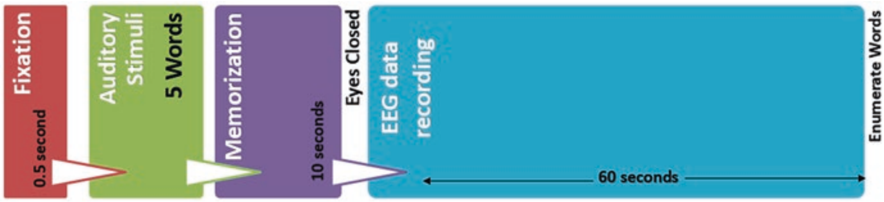

Fig. 14.2 The experimental model of working memory

displays the sociodemographic and cognitive characteristics of the *NC*, *SMCI* and *VD* patients.

The Human Ethics Committee of the *National University of Malaysia* authorized each protocol for an experiment. The participants also completed a consent form to receive information. In this EEG investigation, a session of auditory working memory (WM) test was done. Participants were given a 0.5 second fixation signal at the start of the session and asked to sit as still as possible for the duration of the test. Afterward, as a quick WM test, the participants were given five words to memorize for 10 seconds. Then, while EEG data was being recorded, participants were instructed to close their eyes and think about these words. The patients had to open their eyes once the allotted 60 seconds had passed and make a list of all the words and phrases they had remembered (Fig. 14.2) [3, 29].

14.3.2 Preprocessing Stage

EEG signal preprocessing is required to remove noise, due to the fact that EEG waves typically contain artifacts in the same frequency ranges, allowing for probable overlap with brain processes.

14.3.2.1 Conventional Filters

The *A*/*C* power interference noise was reduced by utilizing a *notch* filter with a 50 *Hz* cut-off frequency [4] and a band-pass filter (*BPF*) with a lower cutoff equating to 3 *dB* at 0.5 *Hz* and an upper cutoff frequency within the range of 64 *Hz*, as described in [69]. In a subsequent step of processing for the filtered EEG dataset, the data were split into 6 trials, with each trial including 10 seconds (6 *x* 10 second periods) and 15360 data points per ten seconds.

14.3.2.2 AICA–WT Technique Methodology

In this study, we present and describe the AICA-WT technique as a fully automatic hybrid approach. The purpose of this strategy is to address the limitations of both ICA and DWT by combining their benefits. To improve the quality of EEG recordings, AICA-WT is applied [75, 76]. ICA is a strong statistical approach for estimating a set of n unknown components, $\mathrm{s}(t) = [s_1(t), \ldots, s_n(t)\ ]$, that were linearly mixed by the ICA linear transform matrix A. The formula is as follows:

$$\mathrm{x}\left(t\right) = \mathrm{As}\left(t\right) \tag{14.1}$$

where the EEGs are denoted by x(t), and both x(t) and s(t) should average out to zero. The demixing matrix W, which is the inverse matrix of A used to represent the linearly ICs, is generated by the ICA from the higher-order statistics of x(t). The ICs can then be determined using Eq. (14.2) (based on the above assumptions) [75, 77, 78]:

$$\mathrm{y}\left(t\right) = \mathrm{Wx}\left(t\right) \tag{14.2}$$

where $\mathrm{y}(t) = [y_1(t), \ldots, y_n(t)\ ]$ is the vector that estimate the ICs

In this investigation, the FastICA algorithm described by Hyvärinen [79] was utilized to decompose EEG signals due to its simplicity, rapid convergence, and efficiency in decomposing the recorded EEG and extracting the new component matrix $\hat{\mathrm{s}}$.

DWT, *symlet* mother wavelet (*MWT*) of *order* 9 '*sym*9', and the *SURE* threshold were chosen to denoise ICA-detected artifacts in a single or many channels [29]. A five-level decomposition of the EEG wave was performed (the sampling rate of the current work was 256 *Hz*). After applying the threshold for each level, the noise on the denoised ICs of the artificial sets was eliminated. Then coefficients were recreated utilizing the inverse *DWT* (*IDWT*). The denoised components have been restored to the initial set of ICs.

The calculated ICA of the original, artifact-free EEG data was then reconstructed as $\hat{\mathrm{x}}$ from the corrected ICs using the following:

$$\hat{\mathrm{x}}(t) = \mathrm{A}\hat{\mathrm{s}}(t) \tag{14.3}$$

where $\hat{s}(t)$ is the new matrix of ICs.

14.3.3 Features Extraction

EEG signals are regarded as a non-invasive, effective diagnostic measure that can provide a more accurate description of emotional state variations across brain regions [21, 23, 80]. Consequently, it is crucial to detect dementia early using EEG signals. The complex dynamics structure of EEG signals can be assessed through the extraction of nonlinear dynamical attributes from the EEGs to identify the most significant features that improve the detection of dementia based on EEG brain mapping [25, 26, 80].

Nonlinear entropy approaches, such as *FuzzEn*, *FDispEn*, and *BubbEn*, have been used to quantify information regarding brain function based on dementia differences. N = 15360 samples and 6 windows of 10 second length (2560 samples) were taken from the EEGs for each of 19 channels over the course of 60 seconds.

14.3.3.1 Fuzzy Entropy (*FuzzEn*)

FuzzyEn has been used to characterize several biomedical data, including electromyograms [81], EEGs, or modulations in the heart rate [19, 20]. Moreover, new research [19] reveals that *FuzzEn* is a reliable entropy estimator for studying biological signals with incomplete data.

Given N data points from a time series $x(n) = x(1), x(2), \ldots, x(N)$, the following algorithm can be used to obtain *FuzzEn* [12]:

1. Create m-vectors $X_m(1), X_m(2), \ldots, X_m(N-m+1)$, where $X_m(i) = [x(i), x(i+1), \ldots, x(i+m-1)] - x0(i)$ for all in the range $1 \le i \le N-m+1$.

   These vectors are a sequence of m consecutive x values, starting at the i^{th} point with the baseline $\left(x_0(i) = \frac{1}{m}\sum_{j=0}^{m-1} x(i+j) \right)$ eliminated.
2. Define the distance between vectors $X_m(i)$ and $X_m(j)$, $d_{ij,m}$, as the biggest absolute difference between their scalar components.
3. Using fuzzy function, determine the similarity degree $D_{ij,m}$ of the vectors $X_m(i)$ and $X_m(j)$ given n and r:

$$D_{ij,m} = \mu\left(d_{ij,m}, r\right) = \exp\left(\frac{-\left(d_{ij,m}\right)^n}{r} \right) \tag{14.4}$$

4. Specify the function φ_m as follows

$$\varphi_m(n,r) = \frac{1}{N-m}\sum_{i=1}^{N-m}\frac{1}{N-m-1}\sum_{j=1,j\neq i}^{N-m} D_{ij,m} \tag{14.5}$$

5. We extend the dimension to $m + 1$, create vectors $X_{m+1}(i)$, and then derive the function $\varphi_{m+1}$by repeating steps 2 through 4.
6. *FuzzEn* can be computed for time series with a finite number of samples N using the following Eq. [81]:

$$FuzEn(m,n,r,N) = \ln\varphi_m(n,r) - \ln\varphi_{m+1}(n,r) \tag{14.6}$$

14.3.3.2 Fluctuation-Based Dispersion Entropy (*FDispEn*)

The entropy metric *DispEn* was developed lately for measuring the randomness of time series. It's fast, and it's performed well in describing time series thus far. In this research, we looked at how different mapping approaches affected *DispEn*'s performance.

The D*ispEn* algorithm is as follows, given a unilabiate signal $x(n) = x(1), x(2), \ldots, x(N)$ of length N:

At the outset, we map $x_j(j = 1, 2, \ldots, N)$ to c classes with indices from 1 to c. $u_j(j = 1, 2, \ldots, N)$ is the signal that has been categorized.

With an embedding dimension m and a time delay of d, we may generate a series of timestamps denoted by $u_i^{m,c}$: $u_i^{m,c} = \left\{u_i^c, u_{i+d}^c, \ldots, u_{i+(m-1)d}^c\right\}, i = 1, 2, \ldots, N-(m-1)d$ [52, 53]. Each dispersion pattern $\pi_{v_0 v_1 \ldots v_{m-1}}$ allocated to the m elements of the vector $u_i^{m,c}$, where $u_i^c = \left\{v_0, u_{i+d}^c = v_1, \ldots, u_{i+(m-1)d}^c = v_{m-1}\right\}$ has a corresponding integer value between 1 and c [52].

The relative frequency for the c^m possible dispersion patterns $\pi_{v_0 v_1 \ldots v_{m-1}}$, is calculated as follows:

$$p\left(\pi_{v_0 v_1 \ldots v_{m-1}}\right) = \frac{\#\left\{\mathrm{i}|, i \le N-1(m-1)d|, u_i^{m,c}\ has\, \pi_{v_0 \ldots v_{m-1}}\right\}}{N-(m-1)d} \tag{14.7}$$

where # means cardinality. $p\left(\pi_{v_0 v_1 \ldots v_{m-1}}\right)$ illustrates the number of *dispersion* patterns of $\pi_{v_0 v_1 \ldots v_{m-1}}$ that is given as $u_i^{m,c}$ divided by the total number of *embedded* signals with *embedding* dimension m.

At last, the *DispEn* value is computed as follows, in accordance with Shannon's notion of entropy:

$$DispEn(x,m,c,d) = -\sum_{\pi=1}^{c^m} p\left(\pi_{v_0 v_1 \ldots v_{m-1}}\right).\ln p\left(\pi_{v_0 v_1 \ldots v_{m-1}}\right) \tag{14.8}$$

In fact, *FDispEn* accounts the variations in behaviour between neighboring elements in adjacent element dispersion patterns, which are based on fluctuation. Thus, we obtain vectors of length $m - 1$ in which every element is a different value between $-c + 1$ and $c - 1$. Thus, there are $(2c - 1)^{m-1}$ potential dispersion patterns based on random fluctuation. The only distinction between the *DispEn* and *FDispEn* algorithms is the potential patterns employed by each technique. Note that the normalized *FDispEn* is represented as [50]

$$\frac{FDispEn}{\ln\left((2c-1)^{m-1}\right)} \tag{14.9}$$

14.3.3.3 Bubble Entropy (*BubbEn*)

BubbEn is created by applying a metric to the permutation approach, which calculates a rough estimate of the work involved in the latter method. Similar vectors are grouped together to reduce the time and effort required to calculate the conditional R'enyi entropy. We limit the number of distinct potential states and generate a coarser distribution based on intrinsic correlations using this method. A sorting algorithm's number of steps is used as the unit of measurement. To determine how many iterations of bubble sort are necessary to sort the vector in ascending order, we count the number of insertions and deletions in the process. We'll call this entropy Bubble Entropy (*BubbEn*). Next, we count the number of swaps $\left(H_{swaps}^{m}\right)$ needed to arrange the vectors in ascending order, and use that information to calculate the conditional R'enyi entropy of this distribution.

$$BubbleEn = \left(H_{swaps}^{m+1} - H_{swaps}^{m}\right) / \log\left(m + 1 / m - 1\right) \tag{14.10}$$

For embedding dimensions m and $\log(1 + m(m + 1)/2)$, respectively, the maximum entropy is $\log\ (1 + m(m - 1)/2)$, and the normalization factor is the difference between these two values. In each case, it indicates how many possible states there are when bubble sort permits swaps between 0 to $m(m - 1)/2$. The state in which no swaps were performed was ignored in order to simplify the normalization factor because it was not relevant for non-zero values of m. The computation of *BubbEn* is shown in pseudo-code below:

1. We use a counting method to determine how many swaps n_i are required to arrange each vector X_i of m elements in in descending order.
2. The probabilities p_i (describing the likelihood of a given number of swaps) n_i are calculated by normalizing the histogram of n_i values by $N - m + 1$.
3. When $\alpha = 2$, the entropy H_{swaps}^{m} swaps is calculated from p_i using the following Equation:

$$H_2(X) = -\log \sum_{i=1}^{n} p_i^2 \tag{14.11}$$

4. Iterating steps 1–3, we find H_{swaps}^{m+1} swaps for vectors with $m + 1$ elements.
5. Using Eq. 14.11, we determine *BubbEn*.

14.3.4 Statistical Analysis

To do ANOVA, the denoising findings, nonlinear entropy feature results of the 19 channels from the EEG datasets of 15 *NC*, 15 *SMCI*, and 5 *VD* patients were preliminarily classified into 5 recording regions that related to the *scalp* region of the cortex. Regionally averaged features aided in taking into account the differences between the scalp regions, which can directly demonstrate the effects of dementia following a stroke in terms of a reduction in brain complexity and a slowing of cognitive function. These regions include the frontal cortex (seven channels: $Fp1$, $Fp2$, $F3$, $F4$, $F7$, $F8$, *and* Fz), the temporal cortex (four channels: $T3$, $T4$, $T5$, *and* $T6$), the parietal cortex (three channels: $P3$, $P4$, *and* Pz), the occipital cortex (two channels: $O1$ *and* $O2$), and the central cortex (three channels: $C3$, $C4$, *and* Cz).

In order to assess the efficacy of the *FuzzEn*, *FDispEn*, and *BubbEn* entropies, three sessions of $two - way$ analysis of variance (*ANOVA*) were statistically analyzed to determine the level of EEG complexity across brain areas. Version 22 of the SPSS program from IBM USA was selected for statistical analysis.

In each of the three sessions, the nonlinear (*FuzzEn*, *FDispEn*, *and BubbEn*) features were dependent variables, whereas the group factor and the five groups of the scalp areas were independent factors. The group factor included *NC* healthy participants, *SMCI* patients who had recently suffered a stroke, and *VD* patients. Then, *Levene's* test for homoscedasticity and the $Kolmogorov - Smirnov$ evaluations for normality were applied. *Duncan's* test was used to determine the $post - hoc$ contrast, and $p < 0.05$ was established as the significance level for each statistical evaluation.

14.3.5 Preliminary Feature Processing Prior Classification

In this work, each EEG channel was divided into 6 epochs, and each epoch was given three entropy features (*FuzzEn*, *FDispEn* and *BubbEn*).

Before being applied to the classifier, the extracted features from the preceding step must undergo additional analysis. The "curse of dimensionality," or difficulties caused by a large number of possible feature combinations, and the resulting increase in processing time can be avoided by employing dimensionality reduction techniques. In order to avoid classifier overload, improve classification model accuracy, and reduce overfitting concerns, this research made use of *dimensionality reduction* techniques. Thus, these solutions are necessary to reduce the dimension of feature vectors.

The dimension of the feature matrix for healthy *NC* and *SMCI* was (90 × 57), (15 *subjects* × 6 *epochs*) = 90 observations and (3 *features* × 19 *channels*) = 57 attributes, whereas for *VD* patients, the dimension was (30 × 57), where (5 *VD* ×6 *epochs*) = 30 observations and (3 *features* × 19 *channels*) = 57 attributes. Therefore, *VD* is an unbalanced set of data that may affect the performance of proposed model. Learning from unbalanced datasets is problematic because the imbalance hinders the performance of the learning algorithms. Given that the *majority* of learning models assume a balanced class distribution, their outcomes tend to favour the dominant *class* whose *class* predictions are inaccurate. Class imbalance in the dataset has a substantial effect on the classification model's precision. However, because the minority class cannot be readily distinguished, the classifier can simply classify each instance as a member of the majority class.

In this study, patients with *VD* serve as an example of the minority class. To rectify the data imbalance, *SMOTE* (Synthetic Oversampling Technique) was employed [82]. In order to reduce *overfitting* and bias in the classification analysis [83], the parameters of the classifier and the amount of oversampling were determined through 10 − *fold* cross-validation and grid search. The supplied dataset was divided into ten distinct subsets of equal size. One of these subsets was used as the test set, while the remaining nine were used to teach the classifier. This method was executed ten times with 10 successful outcomes. The arithmetic mean of these precisions represents the 10 − *fold* cross-validation precision of this dataset's learning algorithm [84].

Because *SMOTE* modifies the dataset, the %age of oversampling has been added to the parameters. Therefore, parameters discovered with various *SMOTE* percentages may not be identical. The *SMOTE* was utilized to balance the class frequency using only the training set [85, 86].

14.3.6 Local Tangent Space Alignment (LTSA)

With its speed and relative insensitivity to parameter choice, the local tangent space alignment (LTSA) method has found widespread application in dimension reduction across a variety of disciplines. In the LTSA method, the coordinates from the local tangent space are combined with the low-dimensional global coordinates using the local radiological transformation matrix. Using the surrounding area as a sample, a tangent space at the local level is constructed. Given the data $x(n) = x(1), x(2), \ldots, x(M) \subset R^{M \times N}$, the, principle of LTSA can be described as following [87]:

1. Create a set X_i consisting of the k nearest neighbors of each sample x_i selected using the k nearest neighbors algorithm, and normalize the results $\hat{X}_i$. It can be written as

$$\hat{X}_i = \left[x_{i,1}, x_{i,2}, \ldots, x_{i,k} \right] \tag{14.12}$$

$$\hat{X}_i = X_i - \overline{x_i} l_k^T \tag{14.13}$$

where $\overline{x_i} = \frac{1}{k} \sum_{j}^{k} x_{i,j}$ and l_k is a unit vector of length k.

2. Perform singular value decomposition to determine the eigenvalues and eigenvectors of the matrix $\hat{X}_i$.

The tangent space H_i is the set of eigenvectors associated with the first d largest singular values.

$$\theta_{ij} = H_i^T \left(x_{ij} - \overline{x_i} \right) \tag{14.14}$$

3. In order to preserve as much data as possible during transformation, we must build the matrix $L_i = \theta_i^+$, where

$$min\mu\left(\gamma\right) = \min \sum_{i=1}^{M} \left| \gamma_i \left(1 - \frac{1}{k} ll^T \right) - L_i \theta_i \right| \tag{14.15}$$

where θ_i^+ represents the generalized inverse matrix of θ_i, Y_i represents the set of nearest neighbors of Y after dimension reduction, that is, $Y_i = (y_{i1}, y_{i2}, \ldots, y_{ik})$.

4. Once the optimization problem in the previous equation has been solved by determining the matrix's eigenvalues and eigenvectors, the embedding matrix Y can be derived. The analogous Equations to (17) are

$$min\mu\left(\gamma\right) = \min\left(YHW\right) = mintr\left(YHW^T H^T Y^T\right), \tag{14.16}$$

$$\left\{ \begin{array}{c} H = \left(H_1, H_2, \ldots, H_M\right) \\ W = diag\left(W_1, W_2, \ldots, W_M\right) \\ W_i = \left(I - \frac{1}{k} ll^T \right)\left(I - \theta_i^+ \theta_i\right) \\ I = YY^T \end{array} \right\}$$

The low-dimensional embedding matrix Y is obtained by computing the eigenvectors that correspond to the second through d^{th} smallest eigenvalues of the alignment matrix B.

$$B = HWW^T H^T \tag{14.17}$$

14.3.7 Dementia Classification Techniques

A thorough analysis of the EEG data was done to classify the individuals' cognitive and mental disability into three groups (NC, *SMCI*, and *VD*). The caliber of the generated features has a significant impact on classifier precision. As a result, the choice of *dimensionality reduction* techniques and the kind of classifier can both have an impact on how accurate the results of the classification are. Three popular methods for categorizing brain illnesses were used in this study: *k*NN, *SVM*, and *DT*.

The parameter k must be specified for the *k*NN classifier. The value of k was altered between 1 and 9 at 2-point intervals. The classifier was trained to determine the optimal value of k, and $k = 5$ was selected empirically. As a measure of similarity for classifying each trial using *k*NN, the Euclidean distance was computed.

Using ten-fold cross-validation to optimize the complexity parameter C with a range of $-4 \le \log_{10}(C) \le 4$ in C values $C \in \{0.0001, 0.001, 0.01, 0.1, 0, 10, 100, 1000, 10000\}$ on the training set produced optimal results for the *SVM* classifier. During testing, C equal to 10 yielded the best outcomes for C values. Based on the radial basis function (*RBF*) kernel, multi-class *SVM* classifiers were implemented. In addition, the training dataset was utilized to calculate the minimum mis-classification rate, which aided in obtaining the smoothing σ value for *SVM* training. The only way to determine the optimal value is by methodically varying during multiple training sessions. As a result, the σ value in this study was changed between 0.1 and 1 at intervals of 0.1. It was determined that a σ value of 0.5 corresponds to the lowest mis-classification rate [19, 22, 28, 32, 44, 88].

In addition, the *DT* classification tree model was utilized. It employs a recursive partitioning algorithm that generates nodes depending on certain criteria for splitting. The produced and divided nodes are then used to grow a tree. To use the split criteria, the optimal split point must be identified. The quality of the splitting criteria is measured by a function derived from the variance function. The optimal point for splitting is determined by a function that is applied to every split point beginning with binary splits and evaluating them based on an optimization criterion. Gini's diversity index has been used as an optimization criterion in this work. When the classification tree reaches the pure node, it stops partitioning the instance space; a node is pure if it contains only observations of one *class* [89]. 50 trees have been employed as the parameter for identifying *VD*, *SMCI*, and *NC* EEG signals using *DT*.

The *performance* of the suggested *framework* was assessed using the *average* classification accuracy reported as a percentage and the confusion matrix, which enabled to determination the effects of dementia recognition enhancement.

14.4 Results and Discussion

Utilizing the novel, 100% automatic AICA-WT denoising technique presented in [19], the EEG dataset was successfully denoised. In our previous investigations [19, 27, 28], we statistically analyzed the differences between the linear spectral distributions of EEG slowing in *VD* patients, *SMCI* patients, and healthy *NC* subjects. The training process is where the most important design decisions for the *k*NN, *SVM*, and *DT* classifiers are made, as they are based on the test set and training set sizes. However, the classifiers employed in this work were trained on the same training data set and assessed on the testing data set in order to compare the performance of the suggested classifiers.

14.4.1 Results of Preprocessing Stage

Compared to the original EEG recording, the artifactual components (red color) were successfully and adequately suppressed (blue color). As depicted in Fig. 14.3, the ocular artifacts were effectively inhibited in *Ch*2 (which represents F8 from the *frontal* region).

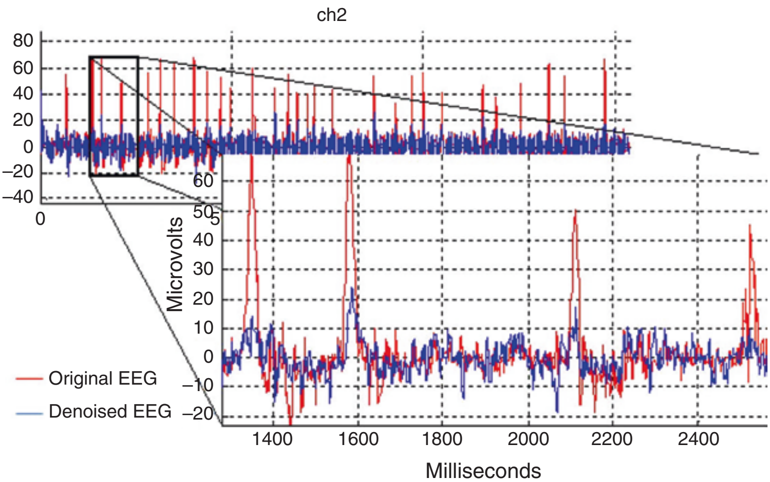

Fig. 14.3 The outcomes of applying the AICA–WT approach to EEG Ch2, which represents F8, to remove ocular artifact

14.4.2 Results of Dementia Recognition by Statistical Analysis

The brain states of *SMCI* patients with *VD* and *SMCI* were distinguished from those of healthy *NC* participants using *FuzzEn*, *FDispEn* and *BubbEn*. Table 14.2 presents a comparative average mean values of the three used entropies which are estimated over five scalp regions for the *VD* patients, *SMCI* patients, and healthy *NC* subjects.

The *VD*s exhibited lower complexity than the *SMCI*s and healthy *NC*s ($FuzzEn_{VaD} < FuzzEn_{MCI} < FuzzEn_{NC}$) with significant differences were observed for the *NC* subjects ($p < 0.05$), ($FDispEn_{VaD} < FDispEn_{MCI} < FDispEn_{NC}$) and ($BubbEn_{VaD} < BubbEn_{MCI} < BubbEn_{NC}$) observable differences were identified between the *VD* patients and the *NC*. In line with expectations, the *complexity* of EEG signals decreases with increasing illness severity, especially in those with *SMCI* and *VD*.

The multiple comparisons have been looked at using the *Bonferroni post hoc* test. The $post - hoc$ dementia multiple comparisons using *Bonferroni* corrections for the *FuzzEn*, *FDispEn*, and *BubbEn* characteristics are displayed in Table 14.3. The *NC* was statistically significant from *VD* ($p = 0.05$) and *SMCI* was statistically significant from *VD* ($p = 0.01$) for the *FuzzEn*, according to post hoc testing using the *Bonferroni* correction.

Additionally, the *SMCI* was statistically significant from *VD* for the *FDispEn* according to post hoc tests with the *Bonferroni* correction ($p = 0.023$).

Additionally, the *post hoc* analyses employing the *Bonferroni* correction for the BubbEn indicated statistically significant differences, especially for *VD*. The statistical difference between the *VD* and the *NC* was 0.05, while the statistical difference between the *VD* and the *SMCI* was 0.003.

Table 14.2 Lists the average values for *FuzzEn*, *FDispEn* and *BubbEn* across all five scalp regions for patients with *VD*, *SMCI*, and *NC* participants. An asterisk indicates differences between groups that are significant

Features	DSC	Frontal	Temporal	Parietal	Occipital	Central	***p***-value
FuzzEn	*NC*	1.147 ± 0.212	1.203 ± 0.171	1.03 ± 0.133	1.236 ± 0.197	1.09 ± 0.171	0.05*
	SMCI	1.08 ± 0.226	1.115 ± 0.264	1.015 ± 0.172	1.086 ± 0.196	1.038 ± 0.205	0.169
	VD	1.079 ± 0.204	1.056 ± 0.191	0.957 ± 0.151	1.073 ± 0.137	0.964 ± 0.254	0.653
FDispEn	*NC*	2.365 ± 0.388	2.514 ± 0.337	2.302 ± 0.243	2.276 ± 0.348	2.525 ± 0.329	0.114
	SMCI	2.333 ± 0.514	2.397 ± 0.524	2.249 ± 0.454	2.228 ± 0.506	2.352 ± 0.477	0.187
	VD	2.222 ± 0.398	2.29 ± 0.332	2.25 ± 0.33	2.111 ± 0.311	2.384 ± 0.302	0.163
BubbEn	*NC*	0.611 ± 0.033	0.609 ± 0.031	0.597 ± 0.027	0.601 ± 0.049	0.609 ± 0.037	0.011*
	SMCI	0.596 ± 0.039	0.592 ± 0.041	0.586 ± 0.046	0.576 ± 0.048	0.579 ± 0.04	0.921
	VD	0.592 ± 0.03	0.59 ± 0.035	0.59 ± 0.043	0.585 ± 0.032	0.593 ± 0.021	0.047*

Table 14.3 *VD*, *SMCI* patients and the *NC* subjects multiple comparison test using *Bonferroni* for *FuzzEn*, *FDispEn* and *BubbEn* entropy features

Dependent Variable	(I) DSC	(J) DSC	Mean Difference (I-J)	***p***-valuea
FuzzEn	*NC*	*SMCI*	−0.036	0.158
		VD	−0.113*	0.05
	SMCI	*VD*	−0.077*	0.01
FDispEn	*NC*	*SMCI*	0.06	0.344
		VD	−0.084	0.358
	SMCI	*VD*	−0.145*	0.023
BubbEn	*NC*	*SMCI*	−0.004	0.709
		VD	−0.020*	0.05
	SMCI	*VD*	−0.016*	0.003

*The mean difference is significant at the 0.05 level

14.4.3 Results of Dementia Recognition by Classification and Performance Measure

Figure 14.4 displays the *confusion matrix* for *VD*, *SMCI* patients and healthy *NC* subjects identification from EEGs using *FuzzEn* with *k*NN, *SVM* and *DT* classifiers, respectively, the correct recognition is observed on the diagonal whereas the off-diagonal represent the substitution errors.

The confusion matrix's two diagonal cells, as shown in Fig. 14.4 using *FuzzEn*, display the %age of correctly classified data from the *k*NN classifier. For instance, 93.33% of the time, *VD* and *SMCI* are correctly categorized. Likewise, all are accurately identified as *NC* subjects (100%) while 5.56% of *VD* are misclassified as *SMCI*, and 1.11% of *VD* and *SMCI* are misclassified as *NC* healthy patients.

Moreover, the *SVM* classifier results show that *VD* and *SMCI* are correctly classified with 64.44% and 97.78%, respectively. Like *NC* subjects, 100% are correctly classified, 28.89% of *VD* are incorrectly classified as *SMCI*, and 6.67% of *VD* and 2.22% of *SMCI* are incorrectly classified as *NC* healthy subjects, respectively.

Additionally, for the *DT* classifier, the confusion matrix shows that the *VD* and *SMCI* are correctly classified with 86.67% and 12.22%, respectively. Similarly, *NC* subjects are correctly classified, whereas 13.33% of *VD* and *SMCI* are incorrectly classified as *NC* healthy subjects. By contrast, 51.11% and 36.67% of *SMCI* are classified as *VD* and *NC* subjects, respectively.

The confusion matrix for *VD*, *SMCI* patients, and healthy *NC* subjects identification from EEG background signals using *DispEn* with *k*NN, *SVM*, and *DT* classifiers, respectively, are presented in Fig. 14.5.

Figure 14.5 illustrates the proportion of correct classification from the *k*NN classifier using *DispEn*. With 97.78% accuracy, *VD* and *SMCI*, whereas *NC* healthy patients are correctly classified with 100%. Similarly, 2.22% of *VD* are wrongly labeled as *SMCI* patients.

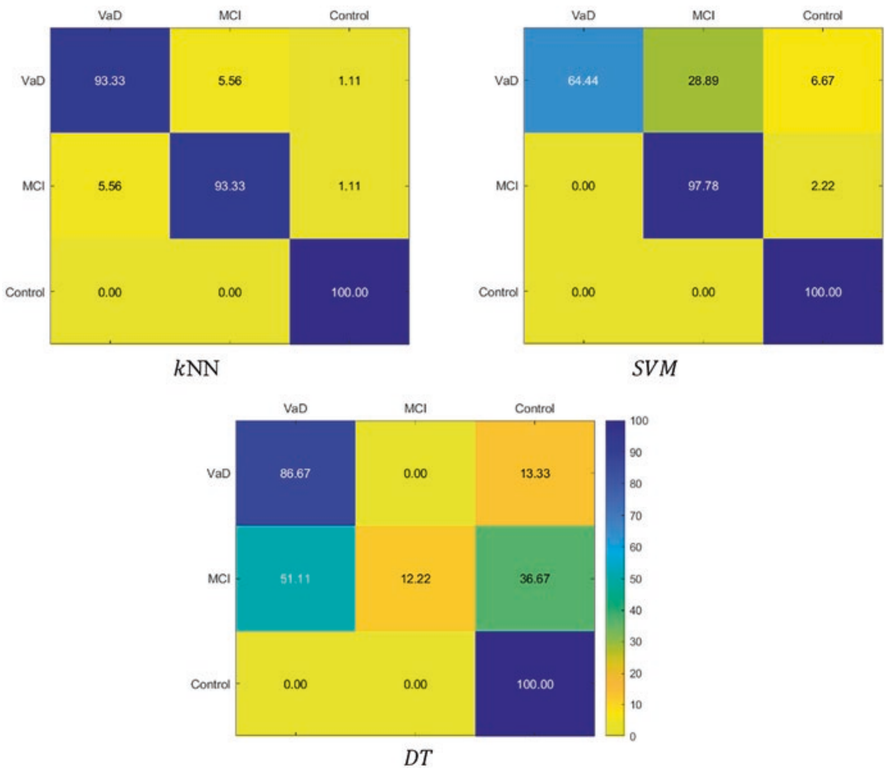

Fig. 14.4 *Confusion matrix* calculations for *VD*, *SMCI*, and *NC* from EEGs using *FuzzEn* and *k*NN, *SVM*, and *DT* classifiers

Furthermore, *VD*, *SMCI* and *NC* are appropriately diagnosed with 98.98%, 95.56% and 100%, respectively, according to the *SVM* classifier results. 1.11% of *VD* are incorrectly classified as *SMCI*, but 4.44% of *SMCI* are wrongly classified as *VD*.

VD are accurately categorized with 18.89%, whereas 81.11% of *VD* are mistakenly labeled as *SMCI* patients and healthy *NC* subjects. Similarly, *SMCI* are accurately classified with 86.67% and 13.33% wrongly labeled as *VD* patients and *NC* subjects, respectively.

NC participants are accurately classified with 91.11% but incorrectly classified as *SMCI* by 8.89%.

Figure 14.6 shows the confusion matrix for identifying *VD*, *SMCI* patients, and healthy *NC* participants from EEG background signals using *BubbEn* with *k*NN, *SVM*, and *DT* classifiers, respectively. On the diagonal, correct recognition is shown, whereas substitution errors are shown off-diagonal.

The proportion of correct classification from the *k*NN classifier utilizing *BubbEn* is shown in Fig. 14.6, *VD* and *SMCI* are correctly categorized with 96.67% accuracy, while *SMCI* and healthy individuals are correctly classified with 100%

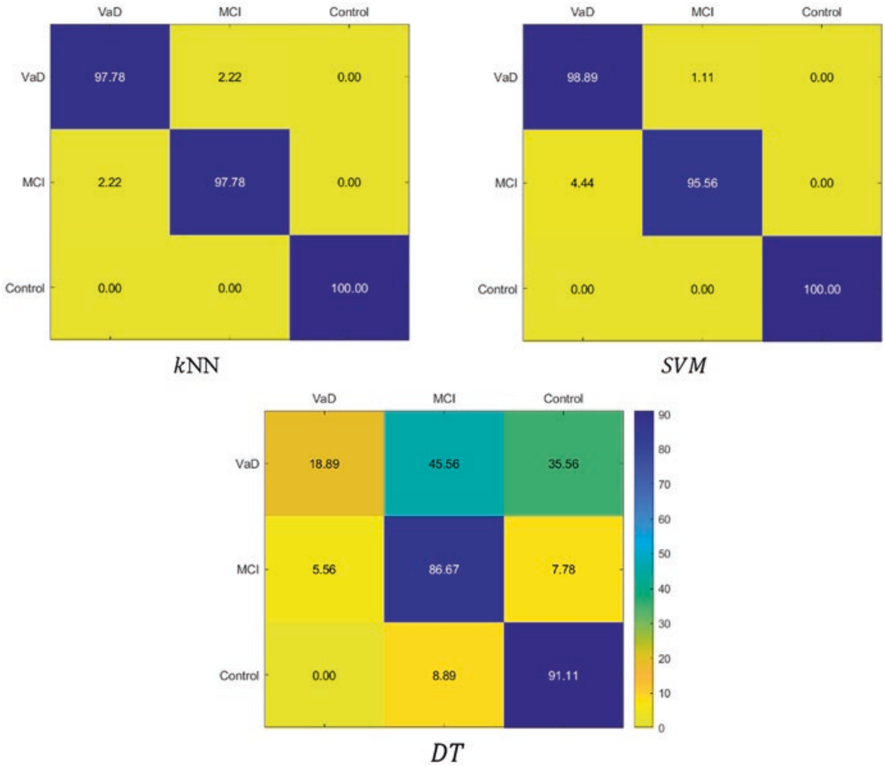

Fig. 14.5 *Confusion matrix* calculations for *VD*, *SMCI*, and *NC* from EEGs using *DispEn* and *k*NN, *SVM*, and *DT* classifiers

accuracy. Similarly, 1.11% and 2.22% of *VD* patients are mistakenly identified as *SMCI* patients and *NC* subjects, respectively.

Furthermore, according to the *SVM* classifier results, *VD*, *SMCI*, and *NC* are correctly diagnosed with 93.33% and 100%, respectively. *VD* is improperly diagnosed as *SMCI* in 1.11% and 5.56% as *NC*.

VD, *SMCI* and *NC* are correctly classified with 82.22%, 80% and 91.11%, respectively. Notably, 17.78% of *VD* are mislabeled as *SMCI* patients and healthy *NC* participants. Similarly, *SMCI* are incorrectly categorized, with only 20% mislabeled as *VD* patients and *NC* participants, respectively. With 8.89% accuracy, *NC* individuals are incorrectly classified as *VD* and *SMCI* patients.

To determine how well the LTSA *dimensionality reduction* technique works with the *k*NN, *SVM*, and *DT* classifiers, a comparative research has been done. The most accurate classifications of *VD*, *SMCI*, and *NC* patients were made using LTSA and *k*NN, in that order. Therefore, the effect of the *FuzzEn*, *FDispEn* and *BubbEn* entropies have been examine without applying the LTSA algorithm individually as shown in Fig. 14.7.

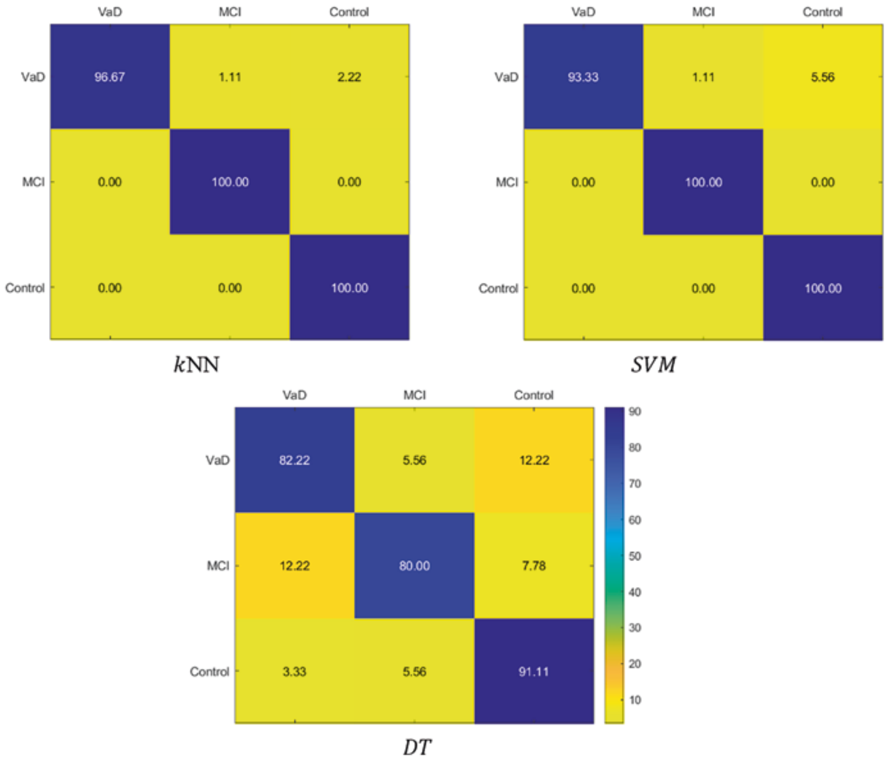

Fig. 14.6 *Confusion matrix* calculations for *VD*, *SMCI*, and *NC* from EEGs using *BubbEn* and *k*NN, *SVM*, and *DT* classifiers

The EEG-based dementia detection framework was evaluated in *MATLAB R*2021*a* on a laptop equipped with a 1.80 *GHz* and 1.99 *GHz* Intel *Core i*7 − 8550*U* processor, 16.0 *GB* of RAM, and a 64 − *bit* operating system.

The comparison of the proposed method with existing methodologies is shown in Table 14.4. Studies have used feature selection and dimensionality reduction techniques to estimate the optimal features. In order to improve the ability to identify *VD* and *SMCI* using EEGs, this study offers an automatic dementia recognition model employing the unique AICA-WT-*BubbEn*-LTSA dementia recognition framework. With the suggested strategy, the classification accuracy of *k*NN, *SVM*, and *DT* has improved somewhat. However, *VD* and *SMCI* recognition from *NC* subjects using the *BubbEn*-LTSA mapping process is the first to be taken into consideration in this study in order to maintain the best quality of features that enhanced the classification accuracy of *VD* and *SMCI* from *NC* subjects. These methods have also been used to study EEGs. Furthermore, the EEG dataset elicitation technique and the EEG estimate system have never been used for securing sensation information, which may make dementia contrasts more clear.

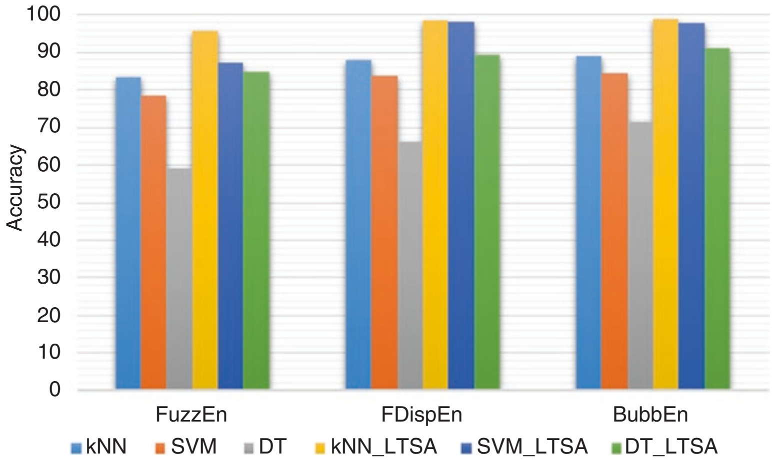

Fig. 14.7 Average accuracy (%) for the *k*NN, *SVM*, and *DT* classifiers as calculated from the *FuzzEn*, *FDispEn* and *BubbEn* entropies with and without using LTSA algorithm

This study has some limitations, including a small sample size and the need for a follow-up analysis with a larger database. Despite this, more research based on real-time online experiments is required to validate the results due to the differences between offline and online categorizations. Despite these caveats, the results of The findings of this study concur with those of other investigations showing that EEG signals can be used to distinguish between those with *VD*, *SMCI* and *NC* [3, 4, 30, 99, 100].

14.5 Conclusion

The pre-processing stage of the EEG datasets of 15 *SMCI* patients had mild cognitive *SMCI*, 15 *NC*, and 5 patients suffering *VD* involved the use of conventional filters and the novel AICA-WT method to denoise the data on WM task. Inh the next stage, the *complexity* and irregularity changes from EEGs have been investigated using the *FuzzEn*, *FDispEn*, and *BubbEn* characteristics. Additionally, the statistical analysis of the EEG complexity across the different brain regions has been done using ANOVA. Then, the nonlinear LTSA dimensionality reduction approach has utilized to enhance the automatic diagnosis of *VD* patients'. *k*-nearest neighbors (*k*NN), support vector machine (*SVM*), and decision tree (*DT*) classifiers have been performed in the final stage. The effectiveness of *FuzzEn*, *FDispEn*, and *BubbEn* have been compared, and the findings demonstrate that *BubbEn* is the technique that consistently separates *VD*, *SMCI* patients, and *NC* from the EEG signals. In order to create the innovative AICA-WT-*BubbEn*-LTSA dementia recognition framework, BubbEn has been chosen to construct a new BubbEn-LTSA mapping approach. The

Table 14.4 Comparative study of the suggested approach to the state-of-the-art

Study	EEG Dataset	Features types	Method	Classifiers	Best Accuracy (%)
Kortelainen et al. [56]	BPF	Frequency domain	SFFS	*k*NN	65
P. Ackermann et al. [61]	BPF	Statistical	mRMR	*SVM*, RF	*SVM* (55)
Al-Qazzaz et al. [45]	Conventional filtering, AICA-WT	*SpecEn*, *ApEn*, *PerEn*	IBGSA	*k*NN	90.52
Al-Qazzaz et al. [44]	SG	*RCMDE*	DEFS_Ch	*SVM*	95.24
H. Cai et al. [90]	BPF, Kalman	*Relative and Absolute* frequency, *Relative and absolute* power, CD, Entropy	*Correlation*-based method, *Wrapper* based method, *PCA*	*SVM* (RBF), RF, LR, *k*NN, *DT*	*DT* (76.4)
H. Cai et al. [91]	FIR, Kalman with DWT, Adaptive-Predictor Filter (APF)	Relative and absolute power, *Hjorth* parameters (*activity*, *mobility*, *complexity*), Shannon Entropy, SE, CD, Peak , Kurtosis, Skewness	Minimal-redundancy-maximal-relevance	*k*NN, *SVM*, *DT*	*k*NN (79.27)
Y. Li et al. [92]	Notch filter, LPF, HPF	AR model + max-power spectrum density, and Sum power, CD, Kolmogorov-Entropy (KE), Shannon Entropy, *PerEn*, LLE, Singular-Value Deposition Entropy (SVDE), Variance, Mean-square (*MS*), Mean of Peak-to-Peak (*P2P*)	Differential evolution	*k*NN	*k*NN (98.40)
H. Peng et al. [93]	BPF	Phase lag index (*PLI*), *alpha*, *beta*, *delta*, *and theta*	Kendall's tau coefficient	*SVM*, KNN, *DT*, NB	*SVM* (92.73)
S. Mahato et al. [94]	BPF	Asymmetry and paired asymmetry of *gamma*1, *gamma*2, *beta*, *alpha*, *theta*, *delta*, DFA, SE	ReliefF	Bagging, *SVM* (kernels such as polynomial,	*SVM* (96.02)

(continued)

Table 14.4 (continued)

Study	EEG Dataset	Features types	Method	Classifiers	Best Accuracy (%)
J. Zhu et al. [95]	LPF, HPF	AR model + Power-Spectrum Density (PSD), AR model + max-power spectrum density, and Sumpower, CD, Kolmogorov-Entropy (KE), Shannon Entropy, *PerEn*, Singular-Value Deposition Entropy (SVDE), Mean-square (MS), Mean of Peak-to-Peak (P2P)	Correlation Feature Selection	LR, *k*NN, RF, *SVM*, BayesNet, *NB*, *J48*	*k*NN (92.65)
R. A. Movahed et al. [96]	LPF, HPF	Synchronization likelihood (SL), Higuchi-Fractal Dimension (HFD), Detrended-Fluctuation Analysis (DFA), CD, Kolmogorov-Entropy (KE), Shannon Entropy, LLE, Kurtosis, Skewness, *DWT*, Relative-Wavelet Energy (*RWE*), Wavelet-Entropy (*WE*)	Sequential Backward Feature Selection (SBFS)	*SVM* (*RBF*), LR, *DT*, *NB*, *RB*, *GB*, *RF*	*SVM* (99)
Narayan et al. [97]	BPF(8 to 30) Hz, notch filter, ICA	CSP	*PCA*	*SVM*, LDA	*SVM* (98.8)
Al-Qazzaz et al. [98]	Emotion	Entropy	*ESD*	*k*NN, *SVM*, RF	*SVM* (87.64)
Our Proposed Method (AICA-WT-*BubbEn*-LTSA)	Conventional filtering, AICA-WT	*FuzzEn*, *FDispEn* and *BubbEn*	LTSA	*k*NN	98.89
				SVM	91.11
				DT	98.89

unique AICA-WT-*BubbEn*-LTSA detection has improved automated *VD* dementia recognition, and it may be a potential framework for enhancing the distinction between *VD* and *SMCI* patients and *NC* participants.

References

1. C. Iadecola et al., Vascular cognitive impairment and dementia: JACC scientific expert panel. J. Am. Coll. Cardiol. **73**(25), 3326–3344 (2019)
2. N.K. Al-Qazzaz et al., Cognitive assessments for the early diagnosis of dementia after stroke. Neuropsychiatr. Dis. Treat. **10**, 1743 (2014)
3. N.K. Al-Qazzaz et al., Cognitive impairment and memory dysfunction after a stroke diagnosis: A post-stroke memory assessment. Neuropsychiatr. Dis. Treat. **10**, 1677 (2014)
4. N.K. Al-Qazzaz et al., Role of EEG as biomarker in the early detection and classification of dementia. Sci. World J. **2014**, 906038 (2014)
5. A.D. Korczyn, V. Vakhapova, L.T. Grinberg, Vascular dementia. J. Neurol. Sci. **322**(1–2), 2–10 (2012)
6. T.B. Cumming, R.S. Marshall, R.M. Lazar, Stroke, cognitive deficits, and rehabilitation: Still an incomplete picture. Int. J. Stroke **8**(1), 38–45 (2013)
7. S. Ankolekar et al., Clinical trials for preventing post stroke cognitive impairment. J. Neurol. Sci. **299**(1–2), 168–174 (2010)
8. A. Cedazo-Minguez, B. Winblad, Biomarkers for Alzheimer's disease and other forms of dementia: Clinical needs, limitations and future aspects. Exp. Gerontol. **45**(1), 5–14 (2010)
9. H. Hampel et al., Biomarkers for Alzheimer's disease: Academic, industry and regulatory perspectives. Nat. Rev. Drug Discov. **9**(7), 560–574 (2010)
10. S.T. DeKosky, K. Marek, Looking backward to move forward: Early detection of neurodegenerative disorders. Science **302**(5646), 830–834 (2003)
11. S.-S. Poil et al., Integrative EEG biomarkers predict progression to Alzheimer's disease at the MCI stage. Front. Aging Neurosci. **5**, 58 (2013)
12. J. Escudero et al., Assessment of classification improvement in patients with Alzheimer's disease based on magnetoencephalogram blind source separation. Artif. Intell. Med. **43**(1), 75–85 (2008)
13. C. Gómez, et al., Magnetoencephalogram background activity analysis in Alzheimer's disease patients using auto mutual information. in *Engineering in medicine and biology society, 2006. EMBS'06. 28th Annual International Conference of the IEEE*. (IEEE 2006)
14. R. Hornero et al., Nonlinear analysis of electroencephalogram and magnetoencephalogram recordings in patients with Alzheimer's disease. Philos. Trans. R. Soc. A Math. Phys. Eng. Sci. **2009**(367), 317–336 (1887)
15. R. Hornero et al., Spectral and nonlinear analyses of MEG background activity in patients with Alzheimer's disease. IEEE Trans. Biomed. Eng. **55**(6), 1658–1665 (2008)
16. P.R. Davidson, R.D. Jones, M.T. Peiris, EEG-based lapse detection with high temporal resolution. IEEE Trans. Biomed. Eng. **54**(5), 832–839 (2007)
17. F. Vecchio et al., Resting state cortical EEG rhythms in Alzheimer's disease: Toward EEG markers for clinical applications: A review. Suppl. Clin. Neurophysiol. **62**, 223–236 (2012)
18. J. Jeong, EEG dynamics in patients with Alzheimer's disease. Clin. Neurophysiol. **115**(7), 1490–1505 (2004)
19. N.K. Al-Qazzaz et al., Automatic artifact removal in EEG of normal and demented individuals using ICA–WT during working memory tasks. Sensors **17**(6), 1326 (2017)
20. P. Nguyen, et al. *Age and gender classification using EEG paralinguistic features*. in *2013 6th International IEEE/EMBS Conference on Neural Engineering (NER)*. IEEE. (2013)
21. N.K. Al-Qazzaz et al., Electroencephalogram profiles for emotion identification over the brain regions using spectral, entropy and temporal biomarkers. Sensors **20**(1), 59 (2020)
22. N.K. Al-Qazzaz, M.K. Sabir, and K. Grammer. *Gender differences identification from brain regions using spectral relative powers of emotional EEG*. in *IWBBIO* 2019 (2019)
23. N.K. Al-Qazzaz, M.K. Sabir, and K. Grammer. *Correlation indices of electroencephalogram-based relative powers during human emotion processing*. in *Proceedings of the 2019 9th international conference on biomedical engineering and technology*. (ACM 2019)

24. N.K. Al-Qazzaz, et al. *Effective EEG channels for emotion identification over the brain regions using differential evolution algorithm*. in *2019 41th annual international conference of the IEEE engineering in medicine and biology society (EMBC)*. (IEEE 2019)
25. Al-Qazzaz, N.K., et al. *Stroke-related mild cognitive impairment detection during working memory tasks using EEG signal processing*. in *2017 fourth international conference on advances in biomedical engineering (ICABME)*. (IEEE 2017)
26. Al-Qazzaz, N.K., et al. *Classification enhancement for post-stroke dementia using fuzzy neighborhood preserving analysis with QR-decomposition*. in *2017 39th annual international conference of the IEEE engineering in medicine and biology society (EMBC)*. (IEEE 2017)
27. N.K. Al-Qazzaz et al., Discrimination of stroke-related mild cognitive impairment and vascular dementia using EEG signal analysis. Med. Biol. Eng. Comput. 56, 137–157 (2018)
28. N.K. Al-Qazzaz, S.H.M. Ali, and S.A. Ahmad. *Comparison of the effectiveness of AICA-WT technique in discriminating vascular dementia EEGs*. in *2018 2nd international conference on BioSignal analysis, processing and systems (ICBAPS)*. (IEEE 2018)
29. N. Al-Qazzaz et al., Selection of mother wavelet functions for multi-channel EEG signal analysis during a working memory task. Sensors **15**(11), 29015–29035 (2015)
30. N.K. Al-Qazzaz et al., Selection of mother wavelets thresholding methods in denoising multi-channel EEG signals during working memory task, in *Biomedical Engineering and Sciences (IECBES), 2014 IEEE Conference on*, (IEEE, 2014)
31. N. Bajaj et al., Automatic and tunable algorithm for EEG artifact removal using wavelet decomposition with applications in predictive modeling during auditory tasks. Biomed. Signal Proc. Control **55**, 101624 (2020)
32. N.K. Al-Qazzaz et al., Discrimination of stroke-related mild cognitive impairment and vascular dementia using EEG signal analysis. Med. Biol. Eng. Comput. **56**(1), 137–157 (2018)
33. S. Xie, S. Krishnan, Wavelet-based sparse functional linear model with applications to EEGs seizure detection and epilepsy diagnosis. Med. Biol. Eng. Comput. **51**(1–2), 49–60 (2013)
34. D. Abásolo et al., Entropy analysis of the EEG background activity in Alzheimer's disease patients. Physiol. Meas. **27**(3), 241 (2006)
35. N.K. Al-Qazzaz, et al. *EEG markers for early detection and characterization of vascular dementia during working memory tasks*. in *Biomedical engineering and sciences (IECBES), 2016 IEEE EMBS conference on*. 2016. (IEEE 2016)
36. N.K. Al-Qazzaz et al., EEG wavelet spectral analysis during a working memory tasks in stroke-related mild cognitive impairment patients, in *International Conference for Innovation in Biomedical Engineering and Life Sciences*, (Springer, 2016)
37. N.K. Al-Qazzaz et al., Entropy-based markers of EEG background activity of stroke-related mild cognitive impairment and vascular dementia patients, in *2nd International Conference on Sensors Engineering and Electronics Instrumental Advances (SEIA 2016)*, (Barcelona, 2016)
38. J. Selvaraj et al., Classification of emotional states from electrocardiogram signals: A nonlinear approach based on Hurst. Biomed. Eng. Online **12**(1), 44 (2013)
39. O. Sourina and Y. Liu. *A fractal-based algorithm of emotion recognition from EEG using arousal-valence model*. in *Biosignals* (2011)
40. N.K. Al-Qazzaz, et al. *EEG markers for early detection and characterization of vascular dementia during working memory tasks*. in *2016 IEEE EMBS Conference on Biomedical Engineering and Sciences (IECBES)*. IEEE (2016)
41. B. García-Martínez et al., Application of entropy-based metrics to identify emotional distress from electroencephalographic recordings. Entropy **18**(6), 221 (2016)
42. N. Thammasan et al., Continuous music-emotion recognition based on electroencephalogram. IEICE Trans. Inf. Syst. **99**(4), 1234–1241 (2016)
43. W.-L. Zheng, J.-Y. Zhu, B.-L. Lu, Identifying stable patterns over time for emotion recognition from EEG. IEEE Trans. Affect. Comput. **10**, 417–429 (2017)
44. N.K. Al-Qazzaz, S.H.M. Ali, and S.A. Ahmad. *Differential evolution based channel selection algorithm on eeg signal for early detection of vascular dementia among stroke survi-*

vors. in *2018 IEEE-EMBS conference on biomedical engineering and sciences (IECBES)*. (IEEE 2018)

45. N.K. Al-Qazzaz et al., Optimal EEG Channel selection for vascular dementia identification using improved binary gravitation search algorithm, in *International Conference for Innovation in Biomedical Engineering and Life Sciences*, (Springer, 2017)
46. A. Freeman et al., Inclusion of sex and gender in biomedical research: Survey of clinical research proposed at the University of Pennsylvania. Biol. Sex Differ. **8**(1), 22 (2017)
47. P. Wang, J. Hu, A hybrid model for EEG-based gender recognition. Cogn. Neurodyn. **13**(6), 541–554 (2019)
48. J. Tian, Z. Luo, Motor imagery EEG feature extraction based on fuzzy entropy. J. Huazhong Univ. Sci. Technol. **41**, 92–95 (2013)
49. Y. Cao et al., *Characterization of complexity in the electroencephalograph activity of Alzheimer's disease based on fuzzy entropy.* Chaos: An interdisciplinary. J. Nonlinear Sci. **25**(8), 083116 (2015)
50. H. Azami, J. Escudero, Amplitude-and fluctuation-based dispersion entropy. Entropy **20**(3), 210 (2018)
51. J.S. Richman, J.R. Moorman, Physiological time-series analysis using approximate entropy and sample entropy. Am. J. Physiol. Heart Circ. Physiol. **278**, H2039–H2049 (2000)
52. M. Rostaghi, H. Azami, Dispersion entropy: A measure for time-series analysis. IEEE Signal Proc. Letters **23**(5), 610–614 (2016)
53. C. Bandt, B. Pompe, Permutation entropy: A natural complexity measure for time series. Phys. Rev. Lett. **88**(17), 174102 (2002)
54. G. Manis, M. Aktaruzzaman, R. Sassi, Bubble entropy: An entropy almost free of parameters. IEEE Trans. Biomed. Eng. **64**(11), 2711–2718 (2017)
55. W. Chen et al., Measuring complexity using fuzzyen, apen, and sampen. Med. Eng. Phys. **31**(1), 61–68 (2009)
56. J. Kortelainen and T. Seppänen. *EEG-based recognition of video-induced emotions: Selecting subject-independent feature set*. in *2013 35th annual international conference of the IEEE engineering in medicine and biology society (EMBC)*. (IEEE 2013)
57. Z. Wang, Z. Zhang, W. Wang, Emotion recognition based on framework of badeba-svm. Math. Probl. Eng. **2019**, 1–9 (2019)
58. H. Ullah et al., Internal emotion classification using EEG signal with sparse discriminative ensemble. IEEE Access **7**, 40144–40153 (2019)
59. B. Nakisa et al., Evolutionary computation algorithms for feature selection of EEG-based emotion recognition using mobile sensors. Expert Syst. Appl. **93**, 143–155 (2018)
60. J. Atkinson, D. Campos, Improving BCI-based emotion recognition by combining EEG feature selection and kernel classifiers. Expert Syst. Appl. **47**, 35–41 (2016)
61. P. Ackermann, et al. *EEG-based automatic emotion recognition: Feature extraction, selection and classification methods*. in *2016 IEEE 18th international conference on e-health networking, applications and services (Healthcom)*. (IEEE 2016)
62. A. Subasi, M. Ismail Gursoy, EEG signal classification using PCA, ICA, LDA and support vector machines. Expert Syst. Appl. **37**(12), 8659–8666 (2010)
63. C. Vidaurre et al., Time domain parameters as a feature for EEG-based brain–computer interfaces. Neural Netw. **22**(9), 1313–1319 (2009)
64. M. Murugappan, N. Ramachandran, Y. Sazali, Classification of human emotion from EEG using discrete wavelet transform. J. Biomed. Sci. Eng. **3**(04), 390 (2010)
65. D. Lagun et al., Detecting cognitive impairment by eye movement analysis using automatic classification algorithms. J. Neurosci. Methods **201**(1), 196–203 (2011)
66. W.A. Chaovalitwongse, Y.-J. Fan, R.C. Sachdeo, On the time series k-nearest neighbor classification of abnormal brain activity. IEEE Trans. Syst. Man Cybern. Part A Syst. Hum. **37**(6), 1005–1016 (2007)

67. D. Abásolo, et al. *Approximate entropy and mutual information analysis of the electroencephalogram in Alzheimer's disease patients*. in *Advances in medical, signal and information processing, 2006. MEDSIP 2006. IET 3rd international conference on* (IET 2006)
68. J. Escudero et al., Analysis of electroencephalograms in Alzheimer's disease patients with multiscale entropy. Physiol. Meas. **27**(11), 1091 (2006)
69. D. Abásolo et al., Approximate entropy and auto mutual information analysis of the electroencephalogram in Alzheimer's disease patients. Med. Biol. Eng. Comput. **46**(10), 1019–1028 (2008)
70. E. Bullmore, O. Sporns, Complex brain networks: Graph theoretical analysis of structural and functional systems. Nat. Rev. Neurosci. **10**(3), 186–198 (2009)
71. X. Jie, R. Cao, L. Li, Emotion recognition based on the sample entropy of EEG. Biomed. Mater. Eng. **24**(1), 1185–1192 (2014)
72. T. Brott et al., Measurements of acute cerebral infarction: A clinical examination scale. Stroke **20**(7), 864–870 (1989)
73. M.F. Folstein, L.N. Robins, J.E. Helzer, The mini-mental state examination. Arch Gen Psychiatry **40**, 812 (1983)
74. T. Smith, N. Gildeh, C. Holmes, The Montreal cognitive assessment: Validity and utility in a memory clinic setting. Can. J. Psychiatr. **52**(5), 329 (2007)
75. J. Escudero, et al., Blind source separation to enhance spectral and non-linear features of magnetoencephalogram recordings. Application to Alzheimer's disease. Med. Eng. Phys., 2009. 31(7): p. 872–879
76. G. Barbati et al., Optimization of an independent component analysis approach for artifact identification and removal in magnetoencephalographic signals. Clin. Neurophysiol. **115**(5), 1220–1232 (2004)
77. C.J. James, C.W. Hesse, Independent component analysis for biomedical signals. Physiol. Meas. **26**(1), R15 (2005)
78. J. Escudero et al., Artifact removal in magnetoencephalogram background activity with independent component analysis. Biomed. Eng. IEEE Trans. **54**(11), 1965–1973 (2007)
79. A. Hyvarinen, Fast and robust fixed-point algorithms for independent component analysis. IEEE Trans. Neural Networks **10**(3), 626–634 (1999)
80. N.K. Al-Qazzaz, et al., *Entropy-Based Markers of EEG Background Activity of Stroke-Related Mild Cognitive Impairment and Vascular Dementia Patients*, in *2nd International Conference on Sensors Engineering and Electronics Instrumental Advances (SEIA'* 2016*)* 2016: Barcelona, Spain. p. 92-94
81. W. Chen et al., Characterization of surface EMG signal based on fuzzy entropy. IEEE Trans. Neural Syst. Rehabil. Eng. **15**(2), 266–272 (2007)
82. N.V. Chawla et al., SMOTE: Synthetic minority over-sampling technique. J. Artif. Intell. Res. **16**, 321–357 (2002)
83. R. Kohavi. *A study of cross-validation and bootstrap for accuracy estimation and model selection*. in *Ijcai*. (1995)
84. Y. Song, J. Zhang, Discriminating preictal and interictal brain states in intracranial EEG by sample entropy and extreme learning machine. J. Neurosci. Methods **257**, 45–54 (2016)
85. I.H. Witten, E. Frank, *Data Mining: Practical Machine Learning Tools and Techniques* (Morgan Kaufmann, 2005)
86. M. Hall et al., The WEKA data mining software: An update. ACM SIGKDD Explorations Newsletter **11**(1), 10–18 (2009)
87. H. Esmaiel et al., Multi-stage feature extraction and classification for ship-radiated noise. Sensors **22**(1), 112 (2021)
88. N.K. Al-Qazzaz, et al. *The role of spectral power ratio in characterizing emotional EEG for gender identification*. In *2020 IEEE-EMBS conference on biomedical engineering and sciences (IECBES)*. (IEEE 2021)
89. S.E. Sánchez-Hernández et al., Evaluation of feature selection methods for classification of epileptic seizure EEG signals. Sensors **22**(8), 3066 (2022)

90. H. Cai et al., Study on feature selection methods for depression detection using three-electrode EEG data. Interdiscip. Sci. Comput. Life Sci. **10**(3), 558–565 (2018)
91. H. Cai et al., A pervasive approach to EEG-based depression detection. Complexity **2018**, 1–3 (2018)
92. Y. Li et al., EEG-based mild depressive detection using differential evolution. IEEE Access **7**, 7814–7822 (2018)
93. H. Peng et al., Multivariate pattern analysis of EEG-based functional connectivity: A study on the identification of depression. IEEE Access **7**, 92630–92641 (2019)
94. S. Mahato et al., Detection of depression and scaling of severity using six channel EEG data. J. Med. Syst. **44**(7), 1–12 (2020)
95. J. Zhu et al., An improved classification model for depression detection using EEG and eye tracking data. IEEE Trans. Nanobioscience **19**(3), 527–537 (2020)
96. R.A. Movahed et al., A major depressive disorder classification framework based on EEG signals using statistical, spectral, wavelet, functional connectivity, and nonlinear analysis. J. Neurosci. Methods **358**, 109209 (2021)
97. Y. Narayan, Motor-imagery EEG signals Classificationusing SVM, MLP and LDA classifiers. TURCOMAT **12**(2), 3339–3344 (2021)
98. N.K. Al-Qazzaz et al., An integrated entropy-spatial framework for automatic gender recognition enhancement of emotion-based EEGs. Med. Biol. Eng. Comput. **60**, 531–550 (2022)
99. N.K. Al-Qazzaz et al., EEG wavelet spectral analysis during a working memory tasks in stroke-related mild cognitive impairment patients, in *International Conference for Innovation in Biomedical Engineering and Life Sciences*, (Springer, 2015)
100. N.K. Al-Qazzaz, et al. *Entropy-based markers of EEG background activity of stroke-related mild cognitive impairment and vascular dementia patients*. in *Sensors and electronic instrumentation advances: proceedings of the 2nd international conference on sensors and electronic instrumentation advances* (2016)